CTLA4 aptamer delivers STAT3 siRNA to tumor-associated and malignant T cells

Andreas Herrmann, … , Marcin Kortylewski, Hua Yu

Technical Advance

Intracellular therapeutic targets that define tumor immunosuppression in both tumor cells and T cells remain intractable. Here, we have shown that administration of a covalently linked siRNA to an aptamer (apt) that selectively binds cytotoxic T lymphocyte–associated antigen 4 (CTLA4[apt]) allows gene silencing in exhausted CD8^{+} T cells and Tregs in tumors as well as CTLA4-expressing malignant T cells. CTLA4 expression was upregulated in CD8^{+} T cells in the tumor milieu; therefore, CTLA4[apt] fused to a STAT3-targeting siRNA (CTLA4[apt]–STAT3 siRNA) resulted in internalization into tumor-associated CD8^{+} T cells and silencing of STAT3, which activated tumor antigen–specific T cells in murine models. Both local and systemic administration of CTLA4[apt]–STAT3 siRNA dramatically reduced tumor-associated Tregs. Furthermore, CTLA4[apt]–STAT3 siRNA potently inhibited tumor growth and metastasis in various mouse tumor models. Importantly, CTLA4 expression is observed in T cells of patients with blood malignancies, and CTLA4[apt]–STAT3 siRNA treatment of immunodeficient mice bearing human T cell lymphomas promoted tumor cell apoptosis and tumor growth inhibition. These data demonstrate that a CTLA4[apt]-based siRNA delivery strategy allows gene silencing in both tumor-associated T cells and tumor cells and inhibits tumor growth and metastasis.

CTLA4 aptamer delivers STAT3 siRNA to tumor-associated and malignant T cells

Andreas Herrmann,[1] Saul J. Priceman,[1] Maciej Kujawski,[1] Hong Xin,[1] Gregory A. Cherryholmes,[1] Wang Zhang,[1] Chunyan Zhang,[1] Christoph Lahtz,[1] Claudia Kowolik,[2] Steve J. Forman,[3] Marcin Kortylewski,[1] and Hua Yu[1]

[1]Department of Cancer Immunotherapeutics and Tumor Immunology, [2]Department of Molecular Medicine, and [3]Department of Molecular Medicine, Beckman Research Institute at City of Hope, Comprehensive Cancer Center, Duarte, California, USA.

Intracellular therapeutic targets that define tumor immunosuppression in both tumor cells and T cells remain intractable. Here, we have shown that administration of a covalently linked siRNA to an aptamer (apt) that selectively binds cytotoxic T lymphocyte–associated antigen 4 (CTLA4[apt]) allows gene silencing in exhausted CD8+ T cells and Tregs in tumors as well as CTLA4-expressing malignant T cells. CTLA4 expression was upregulated in CD8+ T cells in the tumor milieu; therefore, CTLA4[apt] fused to a STAT3-targeting siRNA (CTLA4[apt]–STAT3 siRNA) resulted in internalization into tumor-associated CD8+ T cells and silencing of STAT3, which activated tumor antigen–specific T cells in murine models. Both local and systemic administration of CTLA4[apt]–STAT3 siRNA dramatically reduced tumor-associated Tregs. Furthermore, CTLA4[apt]–STAT3 siRNA potently inhibited tumor growth and metastasis in various mouse tumor models. Importantly, CTLA4 expression is observed in T cells of patients with blood malignancies, and CTLA4[apt]–STAT3 siRNA treatment of immunodeficient mice bearing human T cell lymphomas promoted tumor cell apoptosis and tumor growth inhibition. These data demonstrate that a CTLA4[apt]-based siRNA delivery strategy allows gene silencing in both tumor-associated T cells and tumor cells and inhibits tumor growth and metastasis.

Introduction

Recent promising human results of immunotherapies to block immune checkpoints such as cytotoxic T-lymphocyte–associated antigen 4 (CTLA4) and programmed cell death protein 1 (PD-1) (1–3) illustrate the importance of targeting molecules that inhibit T cell–mediated antitumor immunity. However, the immunosuppressive tumor microenvironment hampers the success of various immunotherapies. There are several intracellular checkpoints with great potential as targets to promote potent antitumor immunity. STAT3, for example, has been shown to be a crucial signaling mediator in tumor-associated immune cells as well as in tumor cells (4–7). In tumor cells, STAT3 promotes tumor cell survival/proliferation, invasion, and immunosuppression (8). In the tumor microenvironment, STAT3 is persistently activated in immune cells, including T cells (9, 10). CD4+ Tregs can induce peripheral tolerance, suppressing CD8+ T cell functions in various diseases, including cancer (6, 11–15). Activated STAT3 in T cells contributes to expanding tumor-associated CD4+ Tregs (6, 16). Moreover, *Stat3*−/− CD8+ T cells, both endogenous and adoptively transferred, mount potent antitumor immune responses compared with those with intact *Stat3* (9).

As a nuclear transcription factor lacking its own enzymatic activity, STAT3 is a challenging target for both antibody and small-molecule drugs (8, 17, 18). Recent pioneering work has shown the feasibility of delivering siRNA into tumor cells in vivo (19). In particular, chimeric RNAs or DNA-RNAs consisting of a siRNA fused to nucleic acid sequences, which bind to either a cell-surface ligand or an intracellular receptor with high affinity, have demonstrated therapeutic efficacy in preclinical models (19–21). The majority of such siRNA delivery technologies involves the fusion of siRNA to an aptamer, a structured RNA with high affinity to epitopes on tumor cells and virally infected epithelial cells. We recently described a technology for efficient in vivo delivery of siRNA into immune cells by linking an siRNA to CpG oligonucleotide, which binds to its cognate receptor, TLR9 (21). TLR9 is expressed intracellularly in cells of myeloid lineage and B cells as well as tumor cells expressing TLR9, including human leukemic cells (21, 22). However, the CpG-siRNA approach does not directly target T cells (21).

Recently, an effective way of delivering siRNA into CD4+ T cells for local treatment of HIV has been developed (20). However, for cancer immunotherapy, it is also crucial to regulate CD8+ effector T cells in addition to CD4+ cells. Further, it is quite plausible that selectively targeting the subpopulations of CD8+ and CD4+ T cells in the tumor microenvironment, rather than T cells in general, should afford more antitumor efficacy while reducing toxicity. The expression of CTLA4 is dysregulated in tumors and in tumor-associated T cells and is a promising immunotherapeutic target (23). The broad antitumor immune response by CTLA4 blockade is thought to be mainly mediated by CD4+ T cells: reducing Tregs and increasing helper T cells (13, 24–27). However, activated/exhausted CD8+ T cells also express CTLA4 (28–30). In this study, we investigate the possibility that a CTLA4[apt] might be able to deliver siRNA into both CD4+ and CD8+ T cells in the tumor milieu and in CTLA4-expressing tumor cells to silence intractable targets.

Results

CTLA4[apt]-siRNA uptake and gene silencing in T cells. We synthesized the CTLA4-targeting aptamer based on published sequences (23) and chemically modified it to protect its biostability (31–33); this was followed by linking it to a mouse STAT3 siRNA (Supplemental Figure 1A; supplemental material available online with this article; doi:10.1172/JCI73174DS1). We tested primary mouse splenic cells to assess specific uptake of the CTLA4 aptamer-STAT3 siRNA (CTLA4[apt]–STAT3 siRNA) in immune cell populations in
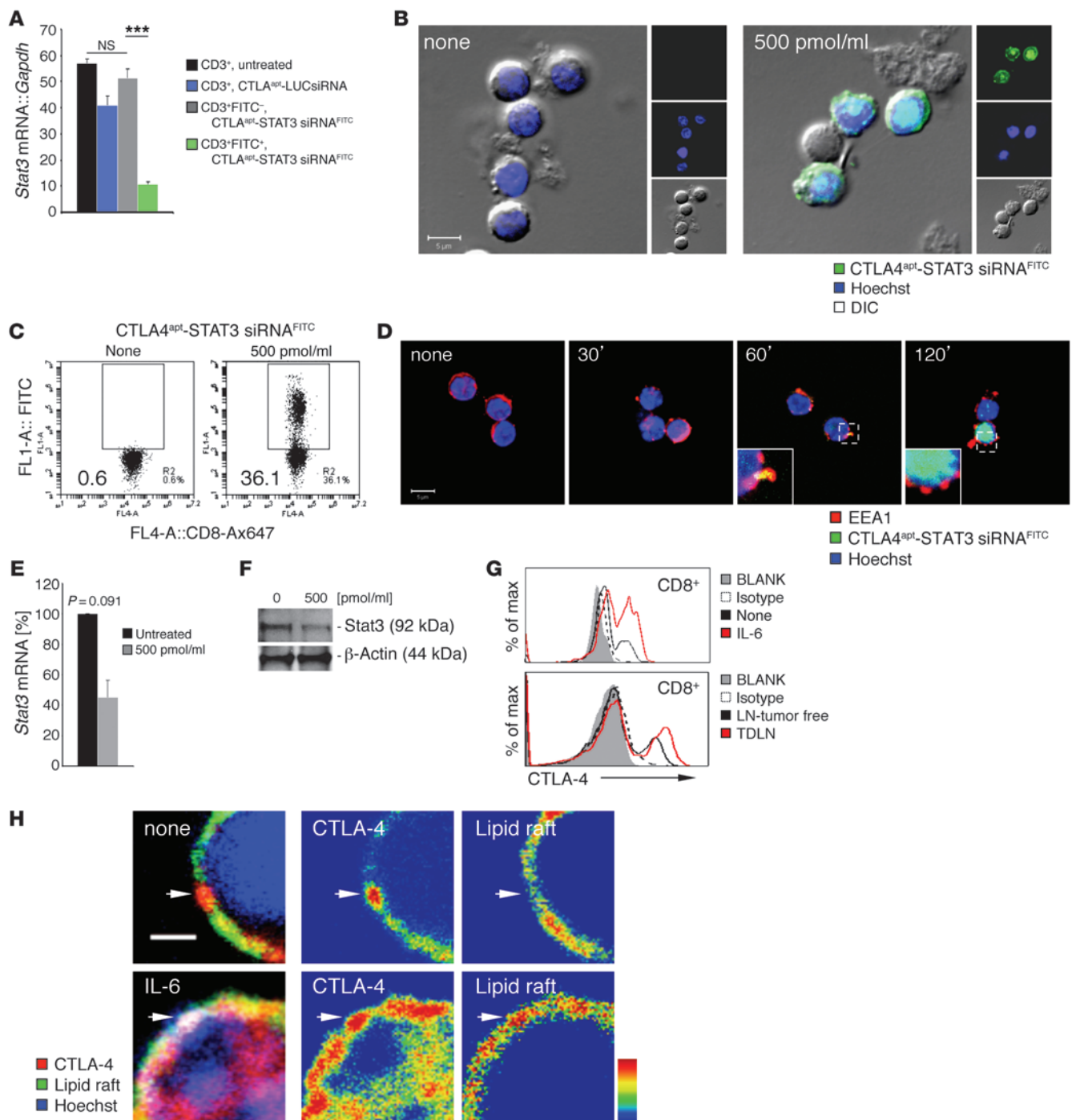
Figure 1

CTLA4apt-siRNA uptake and gene silencing in T cells including CD8+ T cells. (**A**) CTLA4apt-siRNAFITC positive and negative CD3+ T cells were isolated by FACS sorting from tumors of mice (pools of $n = 4$) and treated as indicated. Stat3 mRNA levels were assessed by RT-PCR. SD is shown. ***$P < 0.001$. (**B**) Confocal microscopy indicating CTLA4apt–STAT3 siRNA internalization into CD8+ T cells. Scale bar: 5 μm. Insets were generated in silico by a digital zoom of the indicated regions of interest. (**C**) Uptake of CTLA4apt–STAT3 siRNAFITC by CD8+ cells analyzed by flow cytometry. Gating on CD8+ T cells positive for CTLA4apt–STAT3 siRNAFITC after 2 hours of treatment. (**D**) Intracellular trafficking of CTLA4apt–STAT3 siRNA through endosomal compartments indicated by EEA-1 staining assessed by confocal analysis of CD8+ T cells treated for time points as indicated. Scale bar: 5 μm. Insets were generated in silico by a digital zoom of the indicated regions of interest. (**E**) Stat3 knockdown efficiency in vitro in CD8+ T cells by CTLA4apt–STAT3 siRNA. Stat3 expression analyzed by RT-PCR at RNA level or (**F**) by Western blotting at protein level from CD8+ cell lysates. (**G**) Upregulation of CTLA4 in CD8+ cells stimulated by IL-6 (upper panel) or in the TDLN (lower panel) as analyzed by flow cytometry. (**H**) IL-6 potently stimulates CTLA4 accumulation in lipid rafts. Single-cell suspensions were stained for lipid rafts and CTLA4 upon IL-6 stimulation and analyzed by confocal microscopy (left panel). Lipid raft domains and CTLA4 accumulations in lipid rafts upon IL-6 treatment (white arrowheads) shown in intensity coded false colors (red, high intensity; blue, low intensity; right panels). Scale bar: 2 μm.
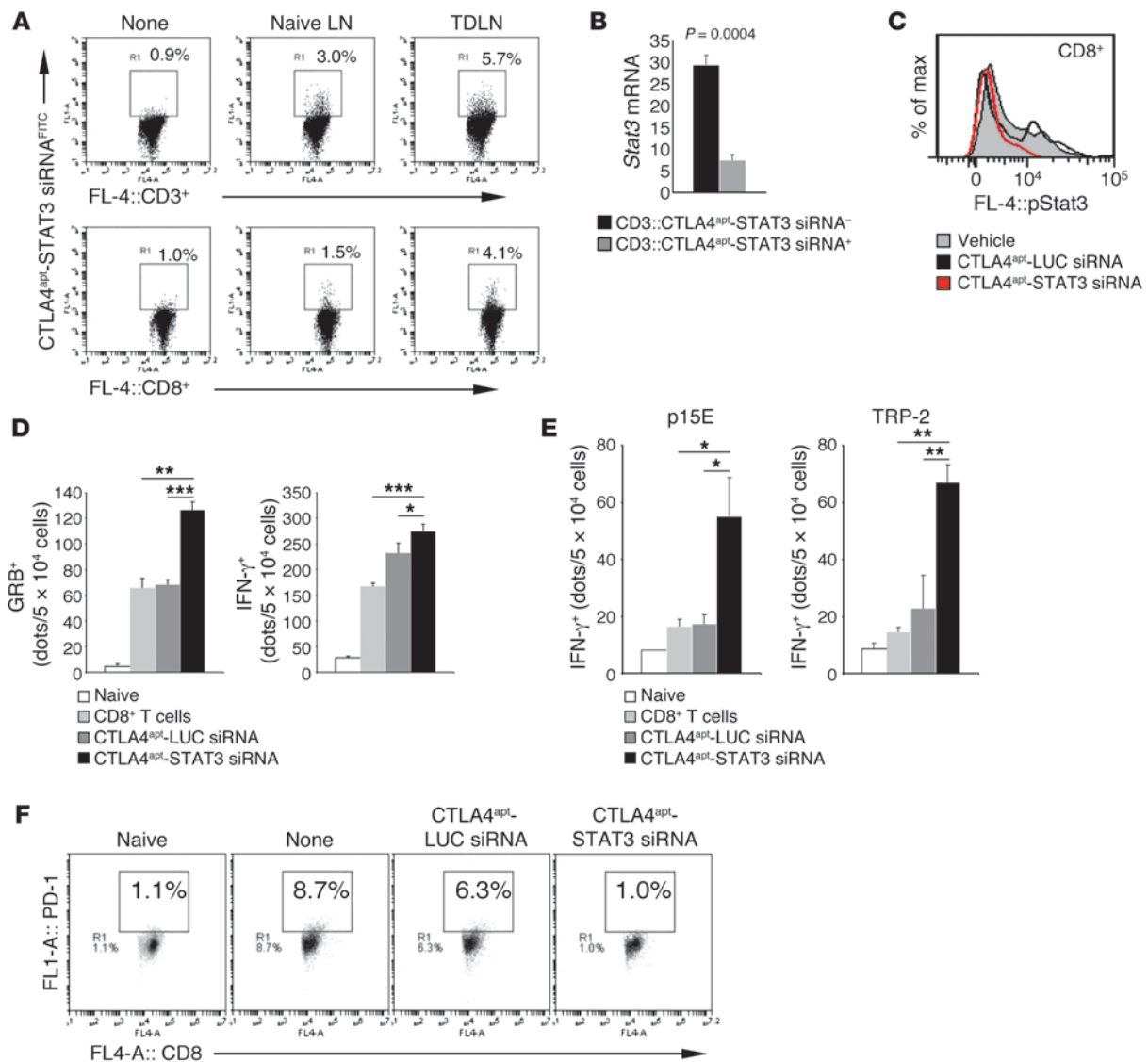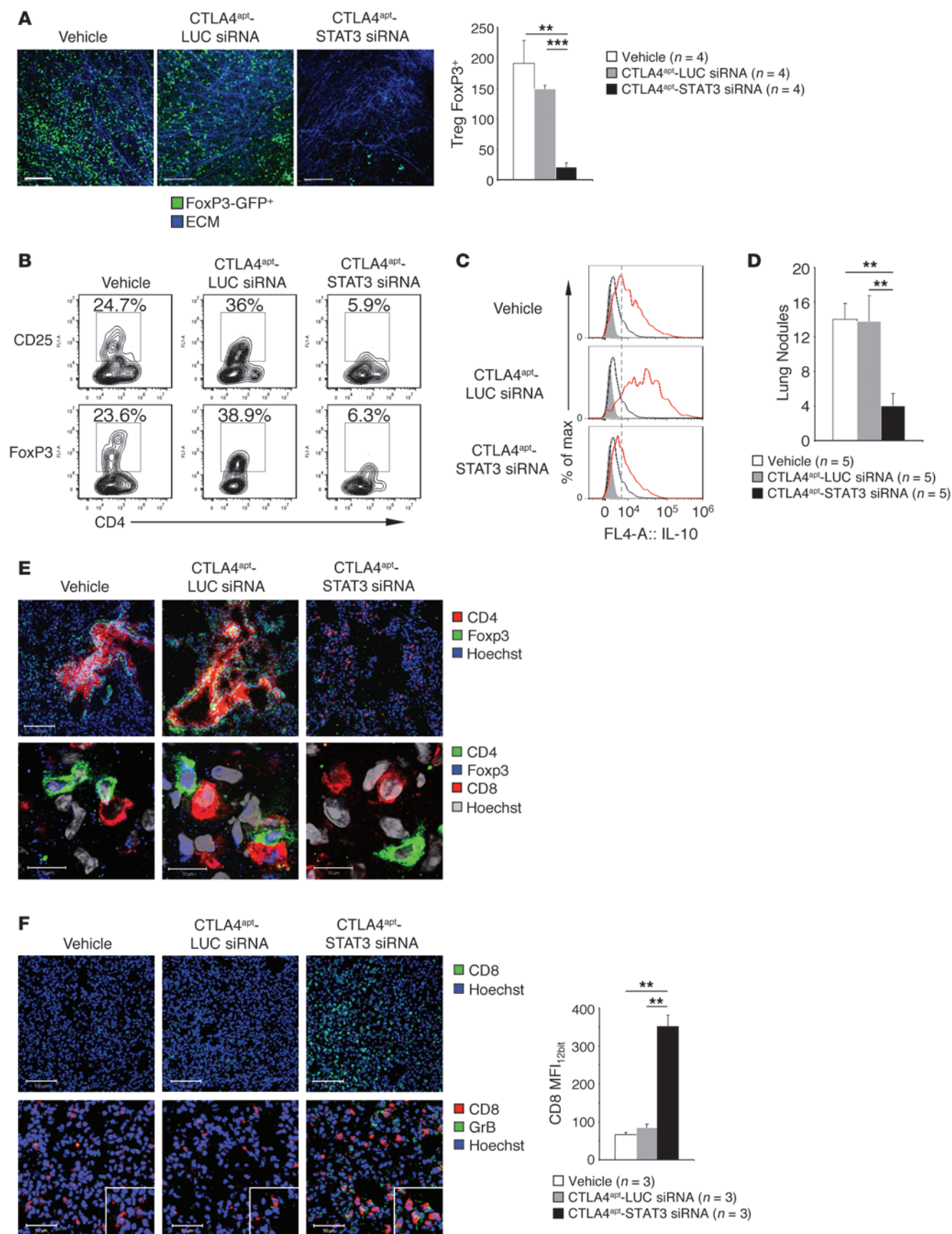
Figure 2

CTLA4[apt]–STAT3 siRNA improves CD8^{+} T cell effector response in vivo. (**A**) In vivo uptake of locally administered CTLA4[apt]–STAT3 siRNA by CD3^{+} and CD8^{+} cells from LNs or TDLNs, respectively. Single-cell suspensions of pooled lymphocytes (n = 3) analyzed by flow cytometry, gating on CTLA4[apt]–STAT3 siRNA[FITC] positive CD3^{+} and CD8^{+} T cells. (**B**) CTLA4[apt]-siRNA[FITC] positive and negative CD3^{+} T cells isolated by FACS sorting from B16 melanoma tumor–bearing mice (all pools: n = 4). Expression of *Stat3* mRNA assessed by RT-PCR. SD and significance are shown. (**C**) In vivo knockdown efficiency by CTLA4[apt]–STAT3 siRNA. Flow cytometric analysis showing pStat3 in CD8^{+} cells from TDLNs after treatment with the indicated siRNA conjugates or control (all pools: n = 4). (**D**) Improved antigen-specific CD8^{+} T cell effector function by CTLA4[apt]–STAT3 siRNA. CD8-OTI cells were adoptively transferred into B16-OVA tumor–bearing *Rag1*^{-/-} mice, followed by CTLA4[apt]–STAT3 siRNA and CTLA4[apt]–LUC siRNA injections (all n = 4). CD8^{+} effector function was assessed analyzing granzyme B (GRB) and IFN-γ in ELISPOT assay. SD is shown. *P < 0.05; **P < 0.01; ***P < 0.001. (**E**) Improved T cell function of lymphocytes isolated from TDLNs after treating B16 melanoma tumor–bearing mice with CTLA4[apt]–STAT3 siRNA or CTLA4[apt]–LUC siRNA (all n = 4). ELISPOT was performed by recalling T cell responsiveness with B16 antigen–specific peptides. SD is shown. *P < 0.05; **P < 0.01, *t* test. (**F**) CD8^{+} T cell exhaustion was assessed by analyzing PD-1 expression upon treating tumor-bearing mice with indicated siRNA conjugates or vehicle control (all pools: n = 4). Gating on PD-1^{+}CD8^{+} T cells.

vitro. Even though CTLA4[apt]–STAT3 siRNA selectively internalized into CTLA4-expressing CD4^{+} and CD8^{+} T cells (Supplemental Figure 1, B–D), macrophages and dendritic cells also took up the chimera in vivo, but to a lesser extent (Supplemental Figure 1E). We then treated a progressive variant of fibrosarcoma tumors (34) with CTLA4[apt]–STAT3 siRNA to assess the silencing efficiency of CTLA4[apt]–STAT3 siRNA in various immune subsets within the

tumor. CD3^{+} T cells, including both CD8^{+} and CD4^{+} T cells that internalized the CTLA4[apt]–STAT3 siRNA (FITC labeled), showed significant *Stat3* gene silencing in vivo (Figure 1A). We isolated CD8^{+} T cells to confirm that CTLA4[apt]-siRNA underwent cellular internalization and exerted a gene-silencing effect. Flow cytometry and live cell confocal microscopy indicated that CD8^{+} T cells internalized CTLA4[apt]-siRNA in vitro (Figure 1, B and C), trafficking

A Vehicle / CTLA4apt-LUC siRNA / CTLA4apt-STAT3 siRNA

Treg FoxP3+

■ FoxP3-GFP+
■ ECM

** / ***

□ Vehicle (n = 4)
■ CTLA4apt-LUC siRNA (n = 4)
■ CTLA4apt-STAT3 siRNA (n = 4)

B Vehicle / CTLA4apt-LUC siRNA / CTLA4apt-STAT3 siRNA

CD25: 24.7% / 36% / 5.9%

FoxP3: 23.6% / 38.9% / 6.3%

CD4

C Vehicle / CTLA4apt-LUC siRNA / CTLA4apt-STAT3 siRNA

% of max

FL4-A:: IL-10

D Lung Nodules

**

□ Vehicle (n = 5)
■ CTLA4apt-LUC siRNA (n = 5)
■ CTLA4apt-STAT3 siRNA (n = 5)

E Vehicle / CTLA4apt-LUC siRNA / CTLA4apt-STAT3 siRNA

■ CD4
■ Foxp3
■ Hoechst

■ CD4
■ Foxp3
■ CD8
■ Hoechst

F Vehicle / CTLA4apt-LUC siRNA / CTLA4apt-STAT3 siRNA

□ CD8
■ Hoechst

■ CD8
■ GrB
■ Hoechst

CD8 MFI$_{12bit}$

**

□ Vehicle (n = 3)
■ CTLA4apt-LUC siRNA (n = 3)
■ CTLA4apt-STAT3 siRNA (n = 3)

Figure 3

CTLA4[apt]–STAT3 siRNA is effective in reducing tumor Tregs. (**A**) CTLA4[apt]–STAT3 siRNA treatments reduce tumor Tregs. FoxP3-GFP+ Tregs were imaged by IVMPM (left panels) in B16 melanoma tumors treated with indicated siRNA conjugates, or control. ECM given by second harmonic generation. Scale bar: 200 μm. GFP+ Tregs are quantified (right panel). SD is shown. **P < 0.01; ***P < 0.001. (**B**) Flow cytometry showing Treg reduction in tumors by CTLA4[apt]–STAT3 siRNA (Tregs were pooled from 4 tumors). Gating on CD25+ and FoxP3+ CD4+ T cells, respectively. (**C**) Flow cytometry analysis showing IL-10 production by tumor Tregs upon indicated treatments. (**D**) Quantification of lung nodules in mice inoculated with melanoma cells and treated with indicated siRNA conjugates systemically. SD is shown. **P < 0.01. (**E**) CTLA4[apt]–STAT3 siRNA systemic treatments reduced lung Treg accumulation and Treg-CD8+ T cell contacts. Scale bars: 100 μm (upper panels); 10 μm (lower panels). (**F**) Confocal microscopy show CTLA4[apt]–STAT3 siRNA treatments increase lung-infiltrating CD8+ T cells and granzyme B+ CD8+ T cells. Scale bars: 100 μm (upper panels); 50 μm (lower panels). Quantification for lung infiltrating CD8+ T cells (right panel). SD is shown. **P < 0.01.

through the endosomal compartment (Figure 1D). Real time RT-PCR and Western blotting further validated target gene silencing in these cells (Figure 1, E and F).

Although CD8+ T cells are known to express low levels of CTLA4, the biological functions of CTLA4 have mainly been characterized in CD4+ Tregs and Th cells (24, 26, 35). We hypothesized that CTLA4 expression might be upregulated in CD8+ T cells in the tumor milieu. Because IL-6 is highly expressed in many tumors including the progressive fibrosarcoma (Supplemental Figure 2, A and B) and was capable of inducing T cell tolerance in the tumor-bearing mice (Supplemental Figure 2, C–J), we tested whether IL-6 could upregulate CTLA4 expression. Flow cytometry showed an increase in CTLA4 protein expression in the tumor-draining LN (TDLN) (Figure 1G), and confocal microscopy revealed that IL-6 treatment led to an accumulation of CTLA4 protein in lipid raft domains (Figure 1, G and H), suggesting a functional redistribution of CTLA4 on the surface of CD8+ T cells (36–38).

CTLA4[apt]–STAT3 siRNA improves CD8+ T cell effector responses in vivo. Using mice bearing B16 melanoma tumors, we first confirmed cellular internalization of CTLA4[apt]–STAT3 siRNA in vivo by CD3+ T cells and their CD8+ subset isolated from TDLNs (Figure 2A). Notably, CTLA4[apt]–STAT3 siRNA uptake by CD8+ T cells was elevated in TDLNs compared with LNs from tumor-free mice, consistent with our hypothesis that tumor milieu/IL-6 upregulated CTLA4 expression, facilitating uptake of the RNA chimera (Figure 2A). Moreover, CTLA4[apt]–STAT3 siRNA administration in vivo resulted in efficient *Stat3* knockdown in T cells compared with CTLA4[apt]–LUC siRNA or vehicle control treatment (Figure 2, B and C). To assess the antigen-specific CTL activity of tumor-associated CD8+ T cells, we adoptively transferred CD8[OT-I] cells into *Rag1*^{−/−} mice bearing B16[OVA] melanoma tumors. Antigen-specific production of granzyme B and IFN-γ by adoptively transferred CD8[OT-I] cells was significantly enhanced upon CTLA4[apt]–STAT3 siRNA treatment compared with treatment with CTLA4[apt]–LUC siRNA, vehicle control, or CD8[OT-I] alone (Figure 2D). Moreover, CTLA4[apt]–STAT3 siRNA treatment of B16 melanoma enhanced antigen-specific adaptive immune responses to endogenous tumor antigens, p15E and TRP-2, compared with CTLA4[apt]–LUC siRNA, vehicle control, or CD8+ T cells alone, as measured by IFN-γ production (Figure 2E). Furthermore, CTLA4[apt]–STAT3 siRNA treat-

ment of B16 tumors reduced PD-1 expression in tumor-associated CD8+ T cells, in contrast with CTLA4[apt]–LUC siRNA or vehicle control treatment (Figure 2F), suggesting an improved CD8+ T cell effector population and an accumulated CTL response in vivo.

CTLA4[apt]–STAT3 siRNA blocks tumor Treg accumulation and inhibits tumor growth. Since tumor-associated FoxP3+ Tregs are a major culprit in tumor-induced immunosuppression and highly express CTLA4 (11), we next tested the effects of CTLA4[apt]-siRNA in targeting this population of T cells. CTLA4[apt]–STAT3 siRNA treatment in Foxp3-GFP B16 tumor–bearing mice resulted in a significant reduction of FoxP3+ Tregs, shown by intravital multiphoton microscopy (Figure 3A). Flow cytometric analysis of CD4+ T cells isolated from tumors of B16 tumor–bearing mice confirmed a reduction in CD4+CD25+FoxP3+ Tregs (Figure 3B). Moreover, since IL-10 is one of the key mediators in suppression of T cell expansion by Tregs and a downstream target gene of STAT3, we evaluated IL-10 production by tumor-infiltrating Tregs. Results from this experiment showed that CTLA4[apt]–STAT3 siRNA could effectively reduce tumor-associated Treg production of IL-10 (Figure 3C). However, monomeric CTLA4[apt] treatment led to increased IL-10 expression that was abolished in vivo upon STAT3 siRNA delivery (Supplemental Figure 3). We further tested whether CTLA4[apt]–STAT3 siRNA could be systemically injected to achieve antitumor effects. Mice with B16 melanoma experimental lung metastases were treated systemically with CTLA4[apt]–STAT3 siRNA, which led to a significant reduction of lung metastasis (Figure 3D). Furthermore, a drastic decrease of CD4+Foxp3+ Tregs was observed, which was accompanied by loss of cell-to-cell contacts of Tregs to CD8+ T cells (Figure 3E). Conversely, infiltration of CD8+ T cells in metastatic lungs was significantly increased upon CTLA4[apt]–STAT3 siRNA treatments (Figure 3F). Lung-infiltrating CD8+ T cells produced more granzyme B, supporting an active antitumor role of CD8+ T cells after systemic treatment of CTLA4[apt]–STAT3 siRNA. In addition, T cells in the lung containing FITC-CTLA4[apt]–STAT3 siRNA are CD3+ (Supplemental Figure 4). The CD8+ subset of these cells had reduced PD-1 expression. (Figure 4A). Moreover, CTLA4[apt]–STAT3 siRNA but not CTLA4[apt]–LUC siRNA uptake induced melanoma antigen–specific CD8+ T cells (Figure 4B) that produce IFN-γ (Figure 4C).

The ability of CTLA4[apt]–STAT3 siRNA to silence Stat3 in both CD8+ and CD4+ T cells in the tumor suggested that CTLA4[apt]–STAT3 siRNA treatment could induce a potent antitumor effect. In order to evaluate its therapeutic efficacy, we administered CTLA4[apt]–STAT3 siRNA, CTLA4[apt]–LUC siRNA, or vehicle control to mice bearing B16 melanoma, Renca renal cell carcinoma, A20 B cell lymphoma, or CT26 colon carcinoma tumors. Results from these experiments showed that CTLA4[apt]–STAT3 siRNA treatments significantly reduced tumor growth in all 4 murine tumor models (Figure 5).

Targeting human CTLA4 to deliver siRNA. The ligand-binding domain of CTLA4 represented by exon 2 coding for amino acids 117–153 harbors the consensus B7-binding motif MYPPPY, which is conserved in mouse and human (Supplemental Figure 5). This prompted us to assess CTLA4[apt] internalization in human CTLA4+ T cell lymphoma cells. Using CTLA4+ Karpas299 T cell lymphoma (Figure 6A), we showed that the same CTLA4[apt] used for siRNA delivery in mouse cells underwent efficient cellular internalization and colocalized with CTLA4 protein in the cytoplasm of the human T cells (Figure 6B). CTLA4+ human T cells efficiently internalize CTLA4[apt]–STAT3 siRNA (Figure 6C), consistent with data shown in normal T cells (Supplemental Figure 1, C and D).
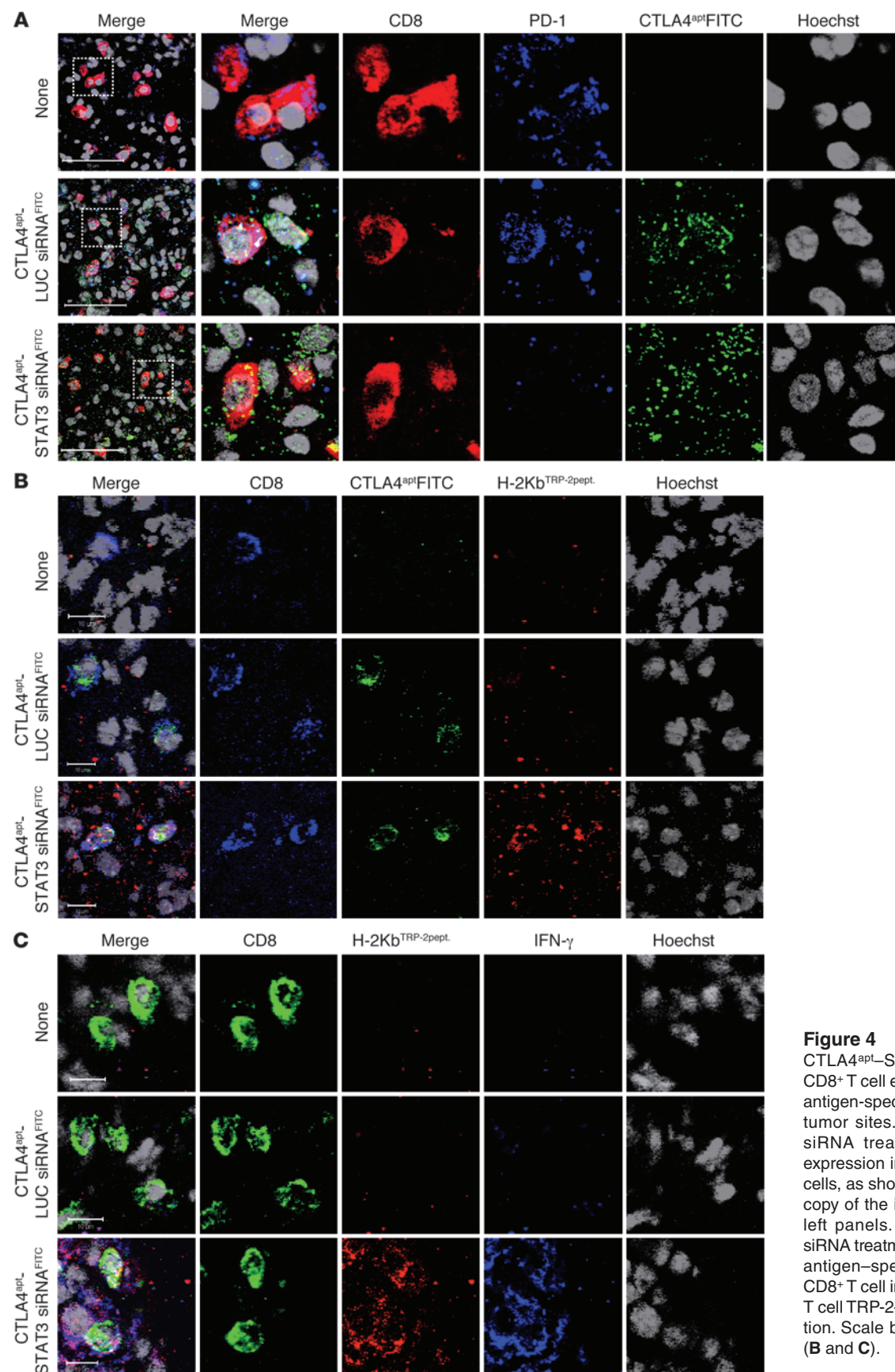
Figure 4
CTLA4apt–STAT3 siRNA prevents CD8+ T cell exhaustion and induces antigen-specific CTLs in secondary tumor sites. (**A**) CTLA4apt–STAT3 siRNA treatments reduce PD-1 expression in lung-infiltrating CD8+ cells, as shown by confocal microscopy of the indicated areas on the left panels. (**B**) CTLA4apt–STAT3 siRNA treatments induce B16 tumor antigen–specific (TRP-2–specific) CD8+ T cell infiltration and (**C**) CD8+ T cell TRP-2–specific IFN-γ production. Scale bars: 50 μm (**A**) 10 μm (**B** and **C**).
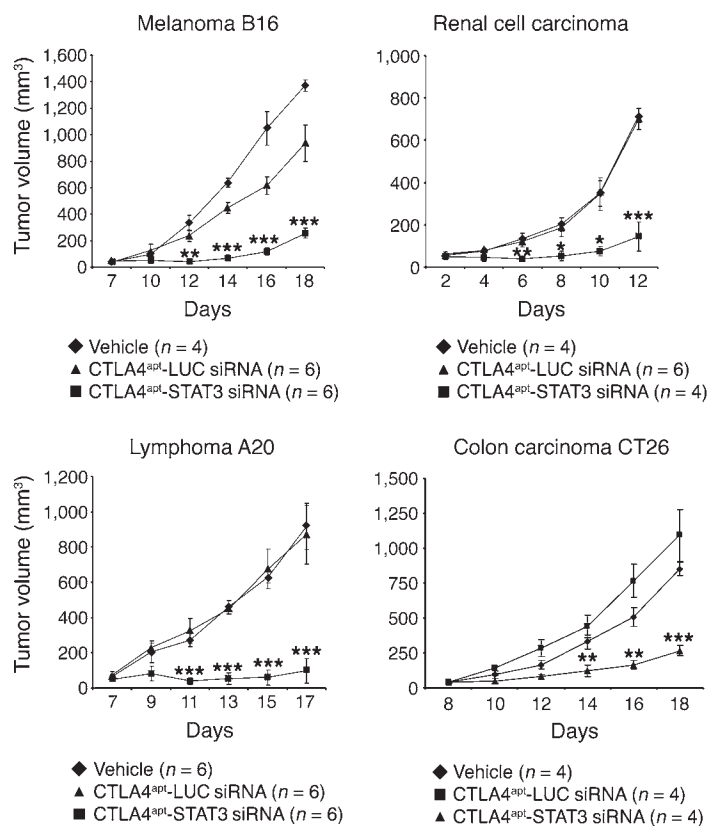
into tumor-associated T cells expressing CTLA4, including exhausted CD8+ T cells and Tregs as well as malignant T cells. CTLA4apt-siRNA treatment enables silencing of intracellular checkpoints that are difficult to target with antibodies and small-molecule drugs. CTLA4apt–STAT3 siRNA treatments improve endogenous adaptive effector functions and induce direct tumor cell killing. While only STAT3 as a therapeutic target in CTLA4-positive cells was tested in the current study, it is anticipated that the CTLA4apt-siRNA conjugates are applicable for other checkpoints and immunosuppressive molecules in tumor-associated T cells and in CTLA4-expressing malignant cells.

Using an antagonistic aptamer recognizing human CD4, Lieberman and colleagues recently demonstrated interrupted HIV transmission and desired RNAi-mediated knockdown of viral genes by CD4apt-siRNA chimeras (20). In these studies, the CD4apt-siRNA conjugate targeted all CD4+ T cell populations, the primary cellular target of HIV. In contrast, the immunosuppressive tumor microenvironment drives CD8+ T cells into exhaustion and promotes Tregs, both of which are associated with expression of inhibitory coreceptors, including CTLA4 and PD-1. Thus, our studies demonstrate the ability to target specific subsets of T cells — tumor-associated CD8+ T cells and Tregs. While its expression is associated with CD8+ T cell exhaustion, CTLA4 intracellular signaling has been reported to possess a broad plasticity of cellular responses ranging from inhibition of cytokine production and blunting clonal expansion to T cell survival (28, 35, 41–43). In our prior investigations, we validated that STAT3 critically contributes to the inhibition of adaptive antitumor immune responses (6, 9). These observations provided a previously unexplored opportunity to selectively target tumor-associated exhausted CD8+ T cell populations to restore effector functions and augment an antigen-specific CTL population by directed *STAT3* gene silencing.

CTLA4apt-siRNA conjugates preferentially undergo cellular internalization in CD4+ and CD8+ T cells. However, the conjugates are also found in macrophages and dendritic cells to a lesser extent, which potentially could support the adaptive antitumor immune response through *STAT3* knockdown in antigen-presenting cells. The uptake by antigen-presenting cells of aptamer-siRNA was also observed in the study using the CD4+ aptamer-siRNA, which seemed to contribute to the efficacy of the chimera in vivo (20). Furthermore, CTLA4apt–STAT3 siRNA treatments, administered locally or systemically, tremendously reduce CD4+CD25+FoxP3+ Treg populations in primary tumors as well as in melanoma lung metastases, indicating modulation of the tumor immunologic environment in favor of an increased antitumor capability by CD8+ T cells. In mouse tumor models, CTLA4apt–STAT3 siRNA administration shows a robust inhibition of tumor growth and metastasis. However, CTLA4apt alone, reported to efficiently block CTLA4, did not improve CTL effector function or impact Treg populations

Furthermore, internalization of CTLA4apt-siRNA by malignant human CTLA4+ T cell lymphoma cells was dose and time dependent, as shown by flow cytometry (Figure 6D). To assess in vivo knockdown efficiency by CTLA4apt-siRNA in human T cell lymphomas, we treated Karpas299luc+ tumors in a xenograft model with CTLA4apt–LUC siRNA. Compared with treatment with CTLA4apt alone, the bioluminescent signal was reduced by over 2-fold upon local administration of CTLA4apt–LUC siRNA (Figure 6E), indicating a specific and robust in vivo target knockdown.

CTLA4apt–STAT3 siRNA inhibits human lymphoma tumor growth. It was previously demonstrated that many types of blood malignancies, including T cell lymphomas, exhibit high CTLA4 expression (39). We therefore tested the feasibility of blocking STAT3 in T cell lymphoma cells with CTLA4apt linking to a human STAT3 siRNA and its potential antitumor effects. Immunohistochemical staining of human T cell lymphoma tissue sections indicated upregulated CTLA4 expression relative to normal LNs (Figure 7, A and B). Treating Karpas299 human T cell lymphoma engrafted in immunodeficient mice resulted in potent tumor growth inhibition (Figure 7C). Tumor growth inhibition was associated with a drastic decrease in STAT3 activation and induction of tumor cell apoptosis (Figure 7D). Additionally, we observed decreased proliferation, reduced tumor vasculature, and reduced B7-H1 expression (Figure 7E).

Discussion
Given the established role of STAT3 in regulating T cell–mediated cancer progression (6, 7, 9, 40), cell-selective targeted therapeutic strategies to inhibit STAT3 activation in T cells are of tremendous interest for future immunotherapies. In the current study, we describe an aptamer-based system to selectively deliver siRNA
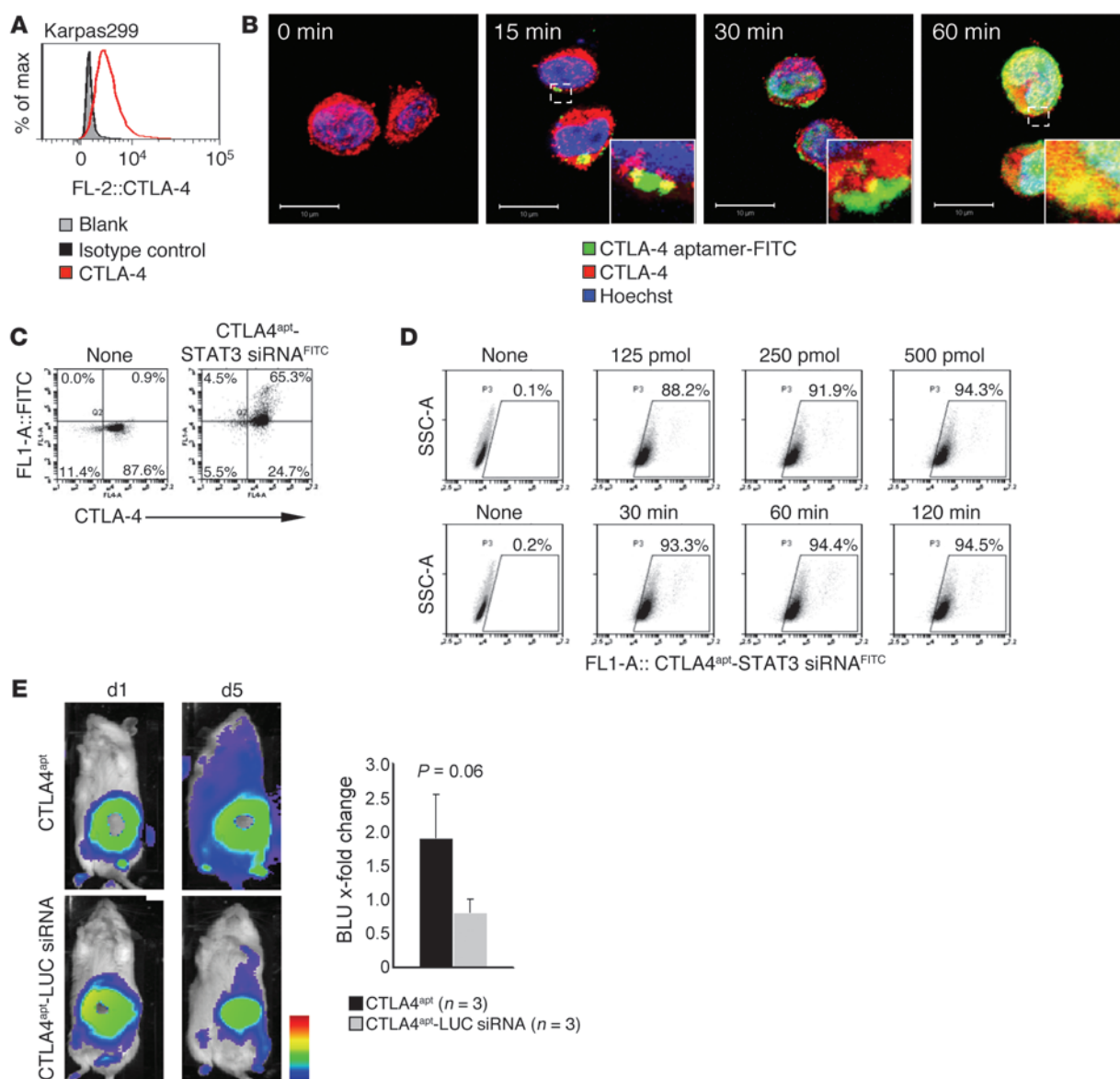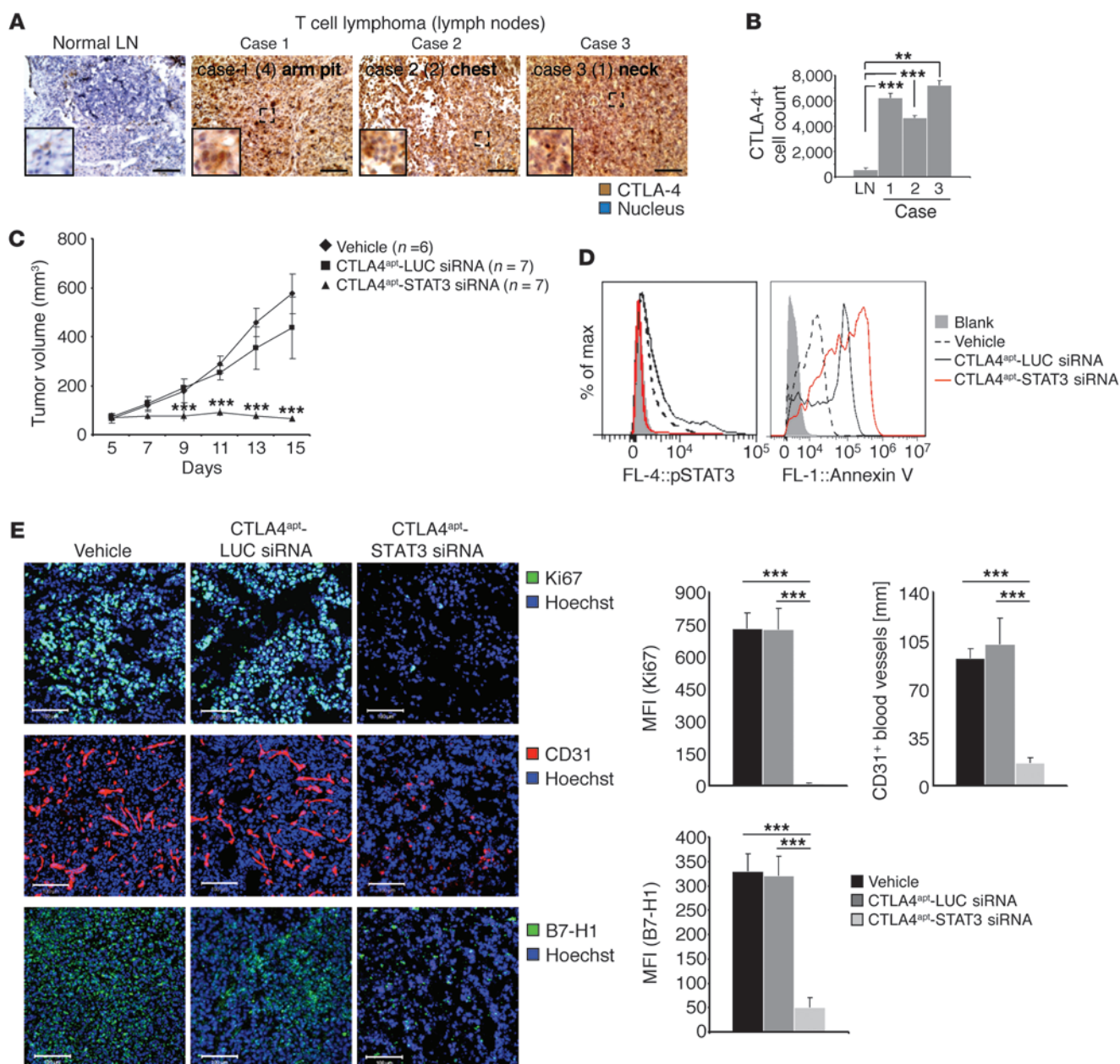
Figure 6
In vivo delivery of CTLA4[apt] conjugate into CTLA4^{+} human T cell lymphoma. (**A**) CTLA4 expression by Karpas299 human T cell lymphoma was assessed by flow cytometry. (**B**) CTLA4[apt] at 500 pmol/ml and CTLA4 protein were analyzed for colocalization in Karpas299 T cell lymphoma cells by confocal microscopy in indicated time kinetics. Scale bars: 10 μm. (**C**) Flow cytometry showing that uptake of the aptamer-siRNA conjugate is more efficient in CTLA4^{+} human T cell lymphoma Karpas cells for 2 hours with 500 pmol/ml CTLA4-[apt]–STAT3 siRNA. Gating on CTLA4^{+} Karpas cells positive for CTLA4[apt]–STAT3 siRNA-FITC (upper right quadrant). (**D**) Flow cytometry analysis showing uptake kinetics of fluorescent CTLA4[apt]–STAT3 siRNA by human Karpas299 T cell lymphoma at indicated doses and time points in vitro. Gating on Karpas cells positive for CTLA4[apt]–STAT3 siRNA-FITC. (**E**) Efficacy of in vivo silencing targeting luciferase. Luciferase[+] Karpas299 tumors engrafted s.c. in immunocompromised mice were treated 3 times every other day with CTLA4[apt]–LUC siRNA or CTLA4[apt] as a control. Bioluminescent noninvasive imaging was performed at time points as indicated, and luminescent signal was quantified (right panel). SD is shown.

in the tumor. This is likely due to the fact that CTLA4[apt] used by Gilboa and colleagues (23) was assembled into tetrameric forms of higher antagonistic activity, while STAT3 siRNA was synthetically fused to a monomeric CTLA4[apt]. However, due to the lethal hyperimmune phenotype of *Ctla4* knockout mice (44, 45) and certain adverse events in patients treated with CTLA4-blocking antibodies (24, 46), an aptamer with additional potent effects antagonizing CTLA4 in the siRNA conjugate may not be necessary.

Besides tumor-associated T cell populations, malignant T cell lymphoma and other blood malignancies also express CTLA4 (47–49). Many of these blood malignancies also display elevated STAT3 activation (50–53). In nonmalignant T cells, CTLA4 oligomerization on the cell surface readily accumulating in the immunological synapse is considered to depend on ligand activation and therefore represents a biologically active form of CTLA4 (36, 54, 55). CTLA4 has also been reported to exist at least dimerized prior to ligation

Figure 7
Treating human T cell lymphoma with CTLA4apt–STAT3 siRNA inhibits tumor growth. (**A**) Human T cell lymphoma tissue array was stained for CTLA4 expression and analyzed by direct immunofluorescence and (**B**) quantified (all $n = 3$). Magnified areas (dashed line) are shown in the lower left corner. Scale bar: 100 μm. Insets were generated in silico by a digital zoom of the indicated regions of interest. SD is shown. **$P < 0.01$; ***$P < 0.001$, t test. (**C**) Tumor growth kinetics of Karpas299 T cell lymphoma engrafted into athymic nude mice treated every other day with CTLA4apt–STAT3 siRNA, CTLA4apt–LUC siRNA, or vehicle. (**D**) Flow cytometry showing phospho-STAT3 expression and apoptotic cell death in the human T cell lymphoma tumors treated as indicated. (**E**) Human T cell lymphoma tumor microsections prepared from mice treated as indicated were stained for Ki67+ proliferative activity (upper panels), CD31+ tumor vasculature (middle panels), and B7-H1+ (lower panels). Scale bars: 100 μm. Fluorescent signals of Ki67 ($n = 5$) and B7-H1 ($n = 4$), and CD31+ ($n = 5$) blood vessel length assessed by confocal microscopy were quantified from independent fields of view; bar graph shows CTLA4apt–STAT3 siRNA (light gray), CTLA4apt–LUC siRNA (dark gray), or vehicle (PBS, black). SD is shown. **$P < 0.01$; ***$P < 0.001$, 2 tailed Student's t test.

(55, 56), indicating the possibility that CTLA4 oligomerizes in a ligand-independent manner in human T cell lymphoma. However, our results indicate that CTLA4apt–STAT3 siRNA efficiently inhibits T cell lymphoma growth concomitant with considerably reduced STAT3 activation. Compared with antagonistic antibodies targeting immune checkpoints, the CTLA4apt-siRNA chimera additionally directly reduces tumor cell growth and tumor immunosuppressive impact on the T cells in the tumor microenvironment.

Methods

Mice and cell culture. For subcutaneous tumor challenge, C57BL/6, *Rag1*(ko) Momj/B6.129S7, *Foxp3*-GFP(ki)/B6, and BALB/c (The Jackson Laboratory) mice were injected with 10^5 B16 melanoma- or ovalbumin-expressing B16^{OVA}, 2.5×10^5 A20 lymphoma, colon carcinoma CT26, or renal clear cell carcinoma (Renca), or 1×10^7 8101 fibrosarcoma regressor or progressor, respectively. For antigen-specific analyses, transgenic OVA TCR (OT-I) mice were obtained from the Jackson Laboratory. Athymic nu/nu mice (National Cancer Institute at Frederick) were engrafted with 10^6 Karpas299 or Karpas299^{luc+} human lymphoma cells s.c. into the flank. After tumors reached 5 to 7 mm in diameter, treatment with 782.5 pmol/dose/mouse CTLA4^{apt} was administered every other day. For experimental induction of metastases by lung colonization, 5×10^4 B16 melanoma cells were injected i.v. via retro-orbital route. Mice that received systemic tumor cell engraftment were treated every other day with 782.5 pmol/dose/mouse CTLA4^{apt} administered i.v. IL-6 depletion was performed using 150 μg/dose injected systemically every other day; cytokine depletion antibodies and IgG control were obtained from BioXCell.

Fibrosarcoma 8101 subclones (gift of Hans Schreiber, Department of Pathology, Cancer Research Center at University of Chicago, Chicago, Illinois, USA) were cultured in DMEM medium (Gibco; Invitrogen) supplemented with 10% FBS (Sigma-Aldrich). Mouse melanoma B16 (provided by Drew Pardoll, The Sidney Kimmel Comprehensive Cancer Center at Johns Hopkins School of Medicine, Baltimore, Maryland, USA) and B16^{OVA} (provided by James J. Mule, H. Lee Moffitt Comprehensive Cancer Center and Research Institute, Tampa, Florida, USA), colorectal adenocarcinoma CT26 (ATCC), renal carcinoma Renca (provided by Alfred Chang, Department of Surgery, University of Michigan, Ann Arbor, Michigan, USA), A20 B cell lymphoma (ATCC), and human Karpas299 T cell lymphoma (ATCC) were grown in RPMI 1640 (Gibco; Invitrogen) containing 10% FBS.

Adoptive T cell transfer and ELISpot assay. B16 or B16^{OVA} cells were injected s.c. into *Rag1*$^{-/-}$ mice, and CD8$^+$ or CD8^{OT-I} T cells (8×10^6 to 10×10^6) and were adoptively transferred via retroorbital route when tumors reached an average diameter of 5 mm. T cells were isolated from spleens and LNs of donor mice using negative selection (EasySep; StemCell Technologies). For antigen-specific responses of CD8$^+$ T cells, 5×10^5 lymphocytes isolated from TDLNs as well as from LNs of naive mice were seeded into a 96-well filtration plate and the CD8$^+$ T cell effector response was recalled using 10 μg/ml peptide (TRP2^{SVYDFFVWL}, OVA^{SIINFEKL} were obtained from AnaSpec; p15E^{KSPWFTTL} was generated by the DNA/RNA and Protein Synthesis Core Facility at City of Hope) for 24 hours at 37°C. Peptide-specific granzyme B and IFN-γ–positive spots were detected according to the manufacturer's instructions (R&D Systems, Diaclone).

Imaging. Indirect immunofluorescence was carried out as described previously (7), staining EEA1, CTLA4, B7-H1 (Santa Cruz Biotechnology Inc.), Hoechst33342 (Sigma-Aldrich), lipid rafts (cholera toxin subunit B; Invitrogen), CD4, IFN-γ, CD31 (BD Biosciences), Foxp3, PD-1, granzyme B, and Ki67 (abcam). H-2Kb-SVYDFFVWL (TRP-2) pentamers were purchased from ProImmune, and tissue staining was carried out according to the manufacturer's instructions. Noninvasive bioluminescent imaging was performed according to the manufacturer's instructions using Ivis 100 (Xenogen). D-Luciferin substrate was obtained from Caliper. In vivo multiphoton microscopy (IVMPM) of melanoma B16 tumors engrafted in C57BL/6 mice expressing GFP under control of the Foxp3 promoter was performed while mice were anesthetized with isoflurane/oxygen. For IVMPM, an Ultima Multiphoton Microscopy System was used (Prairie Technologies). For imaging GFP, the excitation wavelength was set to λ = 890 nm. Band-pass filters optimized for GFP (BP λ = 525/50 nm) were used for detection. Signals of the extracellular matrix were given by second harmonic generation at excitation wavelength λ = 890 nm and were detected with BP λ = 460/50 nm.

Flow cytometry. Cell suspensions and tumor tissues were prepared as described previously (7) and stained with different combinations of fluorophore-coupled antibodies to CD3, CD4, CD8, CD11b, CD11c, CD19, CD25, CD45, F4/80, CTLA4, phospho-Tyr705-Stat3, and IL-10 (BD Biosciences). Annexin V–FITC was purchased from BioVision. Fluorescence data were collected on Accuri (BD Accuri C6) and analyzed using FlowJo software (Tree Star).

Immunoblotting, immunoprecipitation, cytokine array, and ELISA. Whole-cell lysates were prepared using RIPA lysis buffer containing 50 mM Tris (pH 7.4), 150 mM NaCl, 1 mM EDTA, 0.5% NP-40, 1 mM NaF, 15% glycerol, and 20 mM β-glycerophosphate. A protease inhibitor cocktail was added fresh to the lysis buffer (Mini Protease Inhibitor Cocktail; Roche). Normalized protein amounts were subjected to electrophoretic separation by SDS-PAGE and transferred onto nitrocellulose for Western blotting; subsequently, immunodetection was performed using antibodies against CTLA4, STAT3 (Santa Cruz Biotechnology Inc.), and β-actin (Sigma-Aldrich). For coimmunoprecipitation, anti-FITC antibody (Invitrogen) was used to label protein G agarose beads (Invitrogen), which were subsequently incubated for 16 hours with whole-cell lysates, subjected to electrophoretic protein separation and Western blot detection. For determination of cytokine-expression profiles, supernatants of fibrosarcoma 8101Re and 8101Pro were collected from a 24-hour cell culture. Tumor cell supernatants were subjected to cytokine arrays and analyzed according to the manufacturer's instructions (RayBiotech). IL-6 cytokine production by fibrosarcoma 8101Re and 8101Pro was determined from a 24-hour cell culture as described above and analyzed according to the manufacturer's instructions (eBioscience).

PCR and ChIP. Transcript amplification was determined from total RNA purified using RNeasy Kit (QIAGEN). cDNA was synthesized using the iScript cDNA Synthesis Kit (Bio-Rad). Real-time PCR was performed in triplicate using the Chromo4 Real-Time Detector (Bio-Rad). The murine *Gapdh* housekeeping gene was used as an internal control to normalize target gene mRNA levels. Primers were obtained from SA Biosciences (mouse *Stat3*: PPM04643E-200; mouse *Il6*: PPM03015A-200).

ChIP was performed using the ChIP Assay Kit (Upstate Biotechnology) according to the manufacturer's protocol. Briefly, more than 5 million negatively isolated splenic CD8$^+$ T cells pretreated with 20 ng/ml IL-6 (Peprotech) were fixed with 1% formaldehyde at 37°C for 10 minutes and lysed in ChIP-lysis buffer. We incubated the sonicated chromatin solutions with 4 μg of Stat3 antibodies (Santa Cruz Biotechnology Inc.) or with control rabbit IgG. Following immunoprecipitation and reversed crosslinking, DNA was extracted and analyzed by PCR using the following primer sets for mouse PD-1 promoter: 5′-GGATTCCCGTCCCTCGGTCTC-3′ (forward) and 5′-GGGCCAAGGCGCTTGGCACAG-3′ (reverse).

Statistics. Statistical analyses were performed using Prism (Graph-Pad) software. The overall significance for each graph was calculated using 2-tailed Student's *t* test. Data represent average ± SD. *P* values of less than 0.05 were considered statistically significant.

Study approval. Mouse care and experimental procedures with mice were performed under pathogen-free conditions in accordance with established institutional guidance and approved protocols from the Research Animal Care Committees of City of Hope.

Address correspondence to: Hua E. Yu, Department of Cancer Immunotherapeutics and Tumor Immunology, Beckman Research Institute at City of Hope Comprehensive Cancer Center, Duarte, California 91010, USA. Phone: 626.256.4673; Fax: 626.256.8708; E-mail: Hyu@coh.org.

1. Pardoll DM. The blockade of immune checkpoints in cancer immunotherapy. *Nat Rev Cancer*. 2012; 12(4):252–264.
2. Pardoll DM. Immunology beats cancer: a blueprint for successful translation. *Nat Immunol*. 2012; 13(12):1129–1132.
3. Keir ME, Butte MJ, Freeman GJ, Sharpe AH. PD-1 and its ligands in tolerance and immunity. *Annu Rev Immunol*. 2008;26:677–704.
4. Yu H, Pardoll D, Jove R. STATs in cancer inflammation and immunity: a leading role for STAT3. *Nat Rev Cancer*. 2009;9(11):798–809.
5. Kortylewski M, Yu H. Role of Stat3 in suppressing anti-tumor immunity. *Curr Opin Immunol*. 2008; 20(2):228–233.
6. Kortylewski M, et al. Inhibiting Stat3 signaling in the hematopoietic system elicits multicomponent antitumor immunity. *Nat Med*. 2005;11(12):1314–1321.
7. Herrmann A, et al. Targeting Stat3 in the myeloid compartment drastically improves the in vivo antitumor functions of adoptively transferred T cells. *Cancer Res*. 2010;70(19):7455–7464.
8. Yu H, Jove R. The STATs of cancer — new molecular targets come of age. *Nat Rev Cancer*. 2004;4(2):97–105.
9. Kujawski M, et al. Targeting STAT3 in adoptively transferred T cells promotes their in vivo expansion and antitumor effects. *Cancer Res*. 2010; 70(23):9599–9610.
10. Yu H, Kortylewski M, Pardoll D. Crosstalk between cancer and immune cells: role of STAT3 in the tumour microenvironment. *Nat Rev Immunol*. 2007;7(1):41–51.
11. Curiel TJ, et al. Specific recruitment of regulatory T cells in ovarian carcinoma fosters immune privilege and predicts reduced survival. *Nat Med*. 2004; 10(9):942–949.
12. Shevach EM. CD4⁺ CD25⁺ suppressor T cells: more questions than answers. *Nat Rev Immunol*. 2002; 2(6):389–400.
13. Chen ML, et al. Regulatory T cells suppress tumor-specific CD8 T cell cytotoxicity through TGF-β signals in vivo. *Proc Natl Acad Sci U S A*. 2005; 102(2):419–424.
14. Mempel TR, et al. Regulatory T cells reversibly suppress cytotoxic T cell function independent of effector differentiation. *Immunity*. 2006;25(1):129–141.
15. Arens R, Schoenberger SP. Plasticity in programming of effector and memory CD8 T-cell formation. *Immunol Rev*. 2010;235(1):190–205.
16. Pallandre JR, et al. Role of STAT3 in CD4⁺CD25⁺ FOXP3⁺ regulatory lymphocyte generation: implications in graft-versus-host disease and antitumor immunity. *J Immunol*. 2007;179(11):7593–7604.
17. Darnell JE. Validating Stat3 in cancer therapy. *Nat Med*. 2005;11(6):595–596.
18. Darnell JE Jr. Transcription factors as targets for cancer therapy. *Nat Rev Cancer*. 2002;2(10):740–749.
19. McNamara JO 2nd, et al. Cell type-specific delivery of siRNAs with aptamer-siRNA chimeras. *Nat Biotechnol*. 2006;24(8):1005–1015.
20. Wheeler LA, et al. Inhibition of HIV transmission in human cervicovaginal explants and humanized mice using CD4 aptamer-siRNA chimeras. *J Clin Invest*. 2011;121(6):2401–2412.

21. Kortylewski M, et al. In vivo delivery of siRNA to immune cells by conjugation to a TLR9 agonist enhances antitumor immune responses. *Nat Biotechnol*. 2009;27(10):925–932.
22. Zhang Q, et al. TLR9-mediated siRNA delivery for targeting of normal and malignant human hematopoietic cells in vivo. *Blood*. 2013;121(8):1304–1315.
23. Santulli-Marotto S, Nair SK, Rusconi C, Sullenger B, Gilboa E. Multivalent RNA aptamers that inhibit CTLA-4 and enhance tumor immunity. *Cancer Res*. 2003;63(21):7483–7489.
24. Wing K, et al. CTLA-4 control over Foxp3⁺ regulatory T cell function. *Science*. 2008;322(5899):271–275.
25. Byrne WL, Mills KH, Lederer JA, O'Sullivan GC. Targeting regulatory T cells in cancer. *Cancer Res*. 2011;71(22):6915–6920.
26. Peggs KS, Quezada SA, Chambers CA, Korman AJ, Allison JP. Blockade of CTLA-4 on both effector and regulatory T cell compartments contributes to the antitumor activity of anti-CTLA-4 antibodies. *J Exp Med*. 2009;206(8):1717–1725.
27. Lenschow DJ, Walunas TL, Bluestone JA. CD28/B7 system of T cell costimulation. *Annu Rev Immunol*. 1996;14:233–258.
28. Walunas TL, et al. CTLA-4 can function as a negative regulator of T cell activation. *Immunity*. 1994; 1(5):405–413.
29. Teft WA, Kirchhof MG, Madrenas J. A molecular perspective of CTLA-4 function. *Annu Rev Immunol*. 2006;24:65–97.
30. Wherry EJ, et al. Molecular signature of CD8⁺ T cell exhaustion during chronic viral infection. *Immunity*. 2007;27(4):670–684.
31. Connolly BA, Potter BV, Eckstein F, Pingoud A, Grotjahn L. Synthesis and characterization of an octanucleotide containing the EcoRI recognition sequence with a phosphorothioate group at the cleavage site. *Biochemistry*. 1984;23(15):3443–3453.
32. Spitzer S, Eckstein F. Inhibition of deoxyribonucleases by phosphorothioate groups in oligodeoxyribonucleotides. *Nucleic Acids Res*. 1988;16(24):11691–11704.
33. Rettig GR, Behlke MA. Progress toward in vivo use of siRNAs-II. *Mol Ther*. 2011;20(3):483–512.
34. Dubey P, et al. The immunodominant antigen of an ultraviolet-induced regressor tumor is generated by a somatic point mutation in the DEAD box helicase p68. *J Exp Med*. 1997;185(4):695–705.
35. Pandiyan P, et al. CD152 (CTLA-4) determines the unequal resistance of Th1 and Th2 cells against activation-induced cell death by a mechanism requiring PI3 kinase function. *J Exp Med*. 2004;199(6):831–842.
36. Egen JG, Allison JP. Cytotoxic T lymphocyte antigen-4 accumulation in the immunological synapse is regulated by TCR signal strength. *Immunity*. 2002;16(1):23–35.
37. Baroja ML, Madrenas J. Viewpoint: therapeutic implications of CTLA-4 compartmentalization. *Am J Transplant*. 2003;3(8):919–926.
38. Chikuma S, Bluestone JA. CTLA-4 and tolerance: the biochemical point of view. *Immunol Res*. 2003;28(3):241–253.
39. Contardi E, et al. CTLA-4 is constitutively expressed on tumor cells and can trigger apoptosis upon ligand

interaction. *Int J Cancer*. 2005;117(4):538–550.
40. Brayer J, et al. Enhanced CD8 T cell cross-presentation by macrophages with targeted disruption of STAT3. *Immunol Lett*. 2010;131(2):126–130.
41. Linsley PS, et al. Coexpression and functional cooperation of CTLA-4 and CD28 on activated T lymphocytes. *J Exp Med*. 1992;176(6):1595–1604.
42. Linsley PS, et al. Immunosuppression in vivo by a soluble form of the CTLA-4 T cell activation molecule. *Science*. 1992;257(5071):792–795.
43. Madrenas J, et al. Conversion of CTLA-4 from inhibitor to activator of T cells with a bispecific tandem single-chain Fv ligand. *J Immunol*. 2004; 172(10):5948–5956.
44. Tivol EA, et al. Loss of CTLA-4 leads to massive lymphoproliferation and fatal multiorgan tissue destruction, revealing a critical negative regulatory role of CTLA-4. *Immunity*. 1995;3(5):541–547.
45. Waterhouse P, et al. Lymphoproliferative disorders with early lethality in mice deficient in Ctla-4. *Science*. 1995;270(5238):985–988.
46. Leach DR, Krummel MF, Allison JP. Enhancement of antitumor immunity by CTLA-4 blockade. *Science*. 1996;271(5256):1734–1736.
47. Wong HK, et al. Increased expression of CTLA-4 in malignant T-cells from patients with mycosis fungoides — cutaneous T cell lymphoma. *J Invest Dermatol*. 2006;126(1):212–219.
48. Xerri L, Devilard E, Hassoun J, Olive D, Birg F. In vivo expression of the CTLA4 inhibitory receptor in malignant and reactive cells from human lymphomas. *J Pathol*. 1997;183(2):182–187.
49. Kosmaczewska A, Ciszak L, Suwalska K, Wolowiec D, Frydecka I. CTLA-4 overexpression in CD19⁺/ CD5⁺ cells correlates with the level of cell cycle regulators and disease progression in B-CLL patients. *Leukemia*. 2005;19(2):301–304.
50. Scuto A, et al. STAT3 inhibition is a therapeutic strategy for ABC-like diffuse large B-cell lymphoma. *Cancer Res*. 2011;71(9):3182–3188.
51. Holtick U, et al. STAT3 is essential for Hodgkin lymphoma cell proliferation and is a target of tyrphostin AG17 which confers sensitization for apoptosis. *Leukemia*. 2005;19(6):936–944.
52. Sommer VH, et al. In vivo activation of STAT3 in cutaneous T-cell lymphoma. Evidence for an antiapoptotic function of STAT3. *Leukemia*. 2004; 18(7):1288–1295.
53. Liu Y, et al. S1PR1 is an effective target to block STAT3 signaling in activated B cell-like diffuse large B-cell lymphoma. *Blood*. 2012;120(7):1458–1465.
54. Egen JG, Kuhns MS, Allison JP. CTLA-4: new insights into its biological function and use in tumor immunotherapy. *Nat Immunol*. 2002;3(7):611–618.
55. Darlington PJ, Kirchhof MG, Criado G, Sondhi J, Madrenas J. Hierarchical regulation of CTLA-4 dimer-based lattice formation and its biological relevance for T cell inactivation. *J Immunol*. 2005; 175(2):996–1004.
56. Linsley PS, et al. Binding stoichiometry of the cytotoxic T lymphocyte-associated molecule-4 (CTLA-4). A disulfide-linked homodimer binds two CD86 molecules. *J Biol Chem*. 1995;270(25):15417–15424.